The Measurement and Numerical Processing of Chamber Pressures

Allen Dominek and Eddie Dominek

Abstract

An analysis of the chamber pressure is present in context of the position of the bullet. Several strain gauges were mounted along the length of the barrel in this study. Force measurements were also performed to quantify the drag of the bullet as it travels down the barrel. This measurement provides insight to the force required to engrave the bullet which is significant compared to the drag the bullet experiences for majority of the time the bullet is in the barrel.

Keywords: recoil, chamber pressure, measurement, strain gauge, engraving force/drag

1. Introduction

Rifle ballistics are typically focused on the external effects of gravity, wind and drag given an initial muzzle velocity of the bullet. However, there are internal ballistics which determine the muzzle velocity of the bullet. These ballistics are dependent upon the powder (amount and burn rate) and energy losses that the bullet experiences while being released from the neck of the case, entering the bore and traveling through the barrel's bore.

This article addresses the energy losses that are associated with the bullet entering and traveling down the bore. These losses are important since they limit the bullet's muzzle velocity. Overcoming the effects of this energy loss requires a certain amount of the total barrel pressure created by the powder burning. Because of these losses, there is less barrel pressure available to accelerate the bullet.

Measurements of the barrel pressure were performed along the length of a barrel using a Mauser 7x57 cartridge. The barrel pressures are indirectly obtained by measuring the strain along the barrel as the bullet passes through the bore. Strain gauges are placed at several locations along the length of the barrel. The internal pressures then can be related to the measured strain values. The use of a strain gauge for pressure measurements may not be as accurate as would a piezo sensor, but a strain gauge is not as intrusive to the barrel as is a piezo sensor.

The energy losses that a bullet experiences can then be determined through the calculation of the velocity and position of the bullet using measured barrel pressure. One such approach is presented below.

2. Barrel Pressure Acquisition

Inferring internal barrel pressures using strain gauges is well established. Appendix A and Appendix B review this material. Strain measurements were made at four locations along the length of the barrel. Figure 1 illustrates the general locations of the mounted strain gauges on the barrel with their individual Wheatstone bridges and amplifiers. Figure 2 illustrates the chamber geometry and the location of the first strain gauge in relation to chamber and bore lands.

Table 1 provides the location distances of the all the strain gauges with respect to the cartridge base. Figure 3 illustrates a closeup of an amplifier pcb. The voltage amplifier circuit is described in Appendix C. Figure 4 illustrates a closeup of one of the mounted strain gauges. The gauge used was provided by [3] and the gauge model number was CEA-XX-125UN-350. The strain gauges were attached to the barrel using M-200 Bond adhesive and catalyst. This bonding adhesive may not be as good as the permanent M Bond-610 adhesive but the strain gauge is removable with the M-200 Bond adhesive. The output voltages were measured and stored using a Tektronix MDO3104 oscilloscope for post processing.

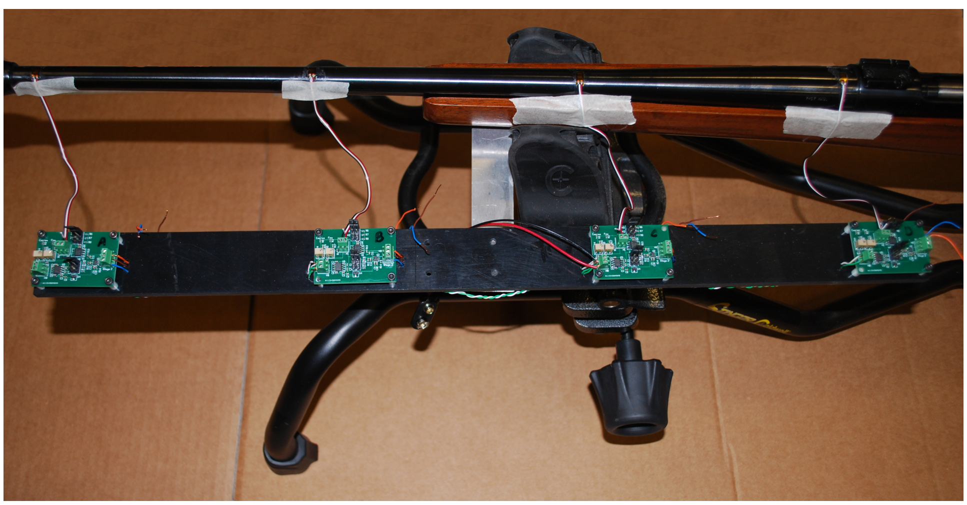

Figure 1: Illustration of the amplifier circuits mounted to the 7mm rifle.

The loads used in this testing were 37 grains of IMR 4320 powder, 46.5 grains and 42 grains of IMR 4350 powder with a Hornady Interlock, 139 grain, 7mm SP bullet. The length of the bullet section, which is .284″ in diameter, is .46″ long as illustrated in Figure 5. The bore length of this barrel is 18.56″. These three loads provided muzzle velocities with averages of 2427, 2598 and 2638 fps, respectively (at chronograph). Consistent data was observed throughout the testing.

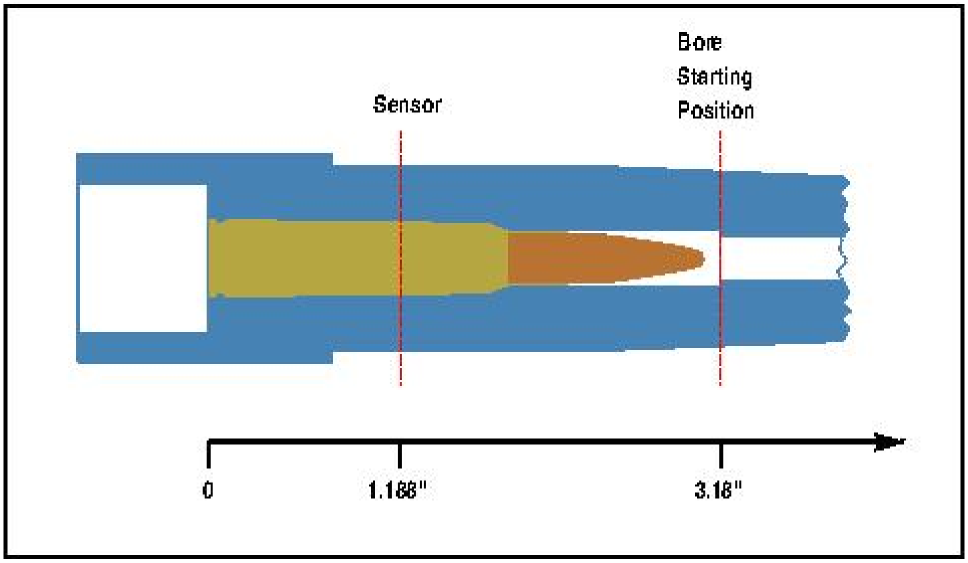

Figure 2: Illustration of chamber geometry and first strain gauge location.

Table 1:

Parameter	Gauge A	Gauge B	Gauge C	Gauge D
Location (inches)	1.095	7.365	13.565	20.083
Barrel r_o (inches)	.5685	.37	.3225	.279
Barrel r_i (inches)	.1135	.1135	.1135	.1135
Casing r_o (inches)	.1135			
Casing r_i (inches)	.0935			
Gain	2582	2562	2589	2581
Young's Modulus (steel)	$30. * 10^6$	$30. * 10^6$	$30. * 10^6$	$30. * 10^6$
Young's Modulus (brass)	$16. * 10^6$			

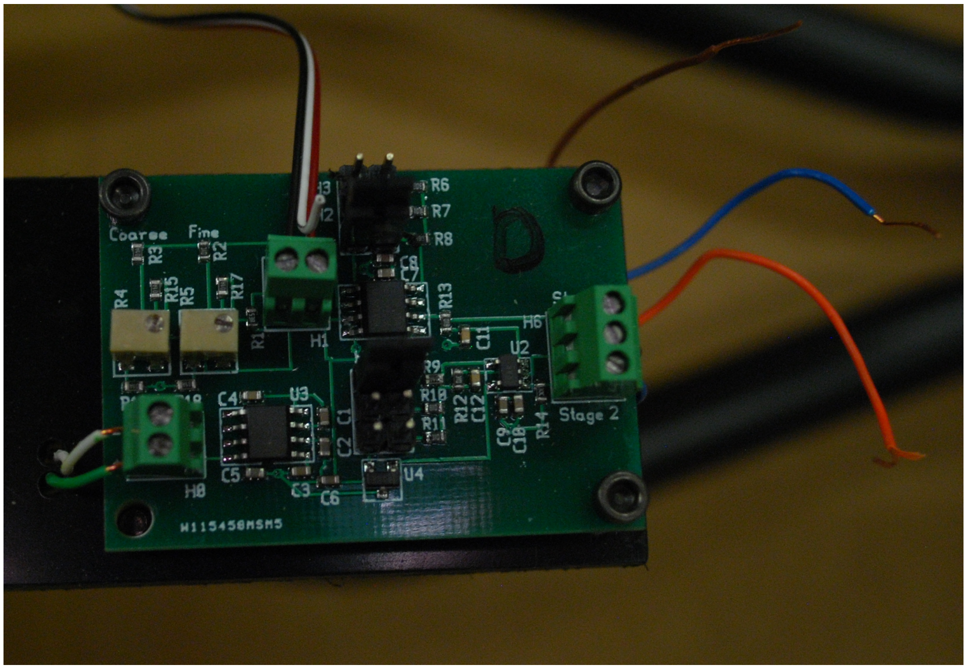

Figure 3: Closeup of an amplifier circuit.

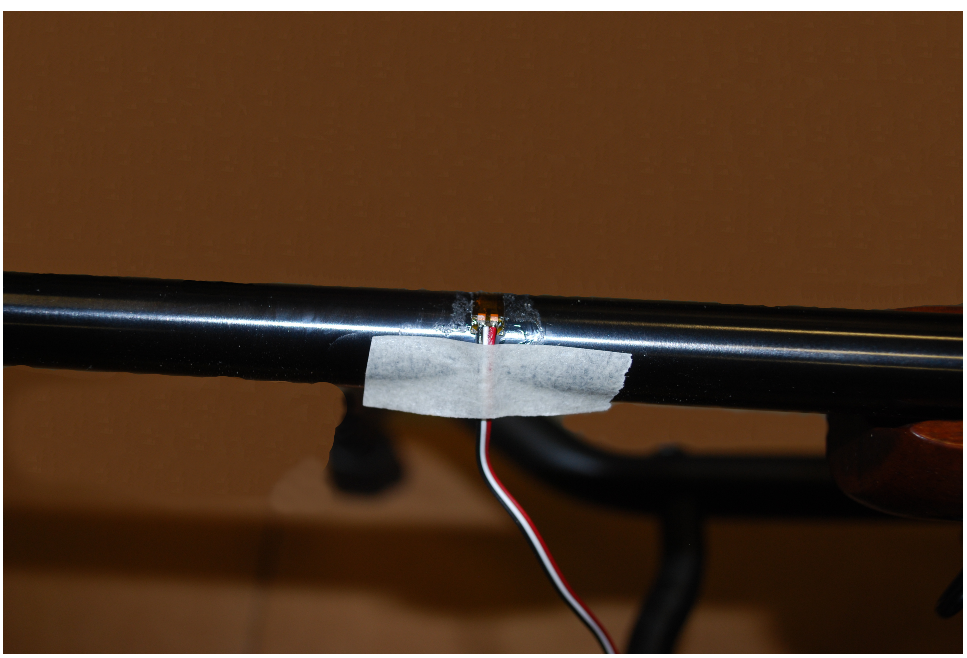

Figure 4: Closeup of a mounted strain gauge.

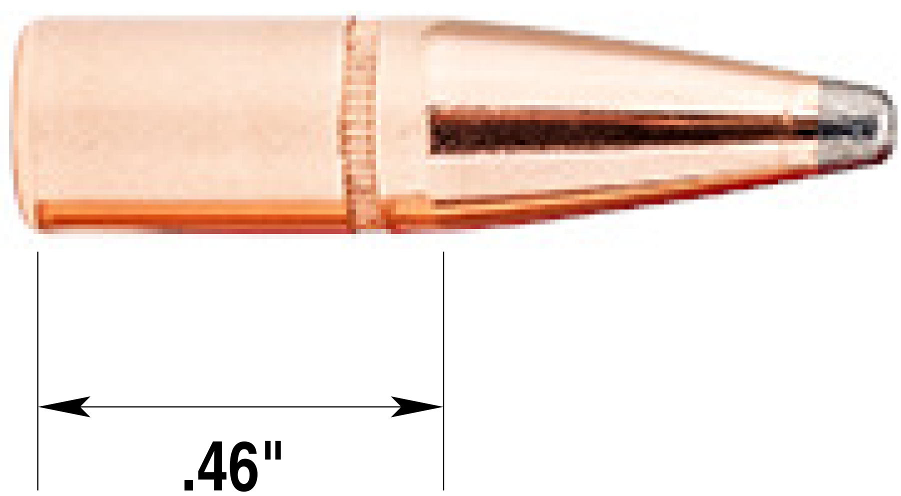

Figure 5: Illustration of a Hornady 7mm Interlock SP bullet showing the region of constant bullet diameter (.46″).

3. Data Processing

Strain gauge voltage measurements were taken for several shots. The measured voltages were consistent with a standard deviation of 40 fps for the measured muzzle velocities.

Initial measurements obtained data from all four strain gauges. However, the data from the strain gauge next to the muzzle is not shown since in some cases there was a hardware issue. The late time response for this gauge was adversely affected by the shock wave generated by the muzzle brake. The timing data from this gauge was not required for the desired signal processing.

The measured data was processed using the equations presented in the appendices to numerically derive the pressure, velocity and distance values. Figures 6 through 11 illustrate measured voltages and calculated pressures from the strain gauges for the three loads. Note that there is a rise in pressure near the end of the barrel. This is most likely due to a muzzle brake that was installed. The installation of this muzzle break may have constricted the bore slightly. Table 2 contains various parameters from the measured data.

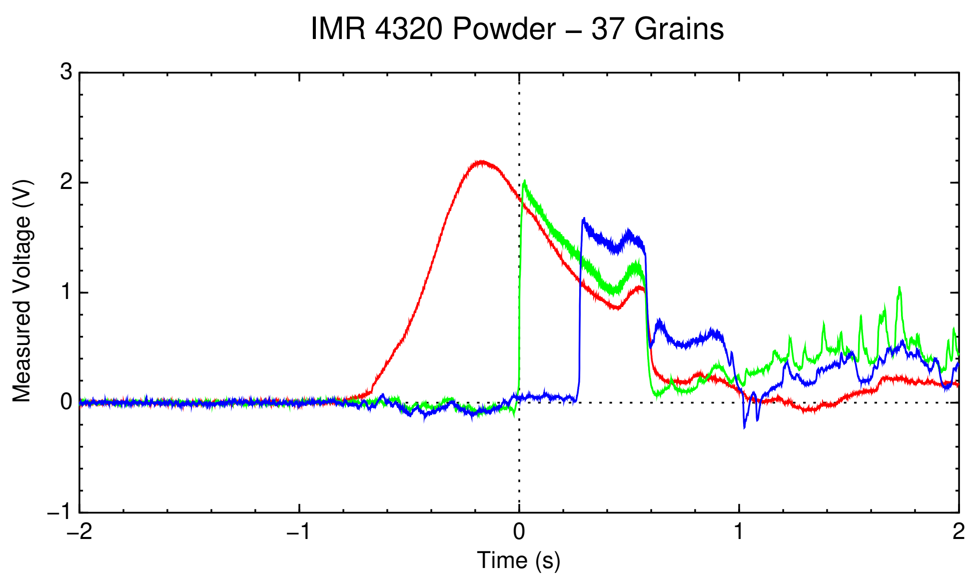

Figure 6: Measured voltages. Positions from base of case: Red-1.188″, Green-7.443″, Blue-13.653″.

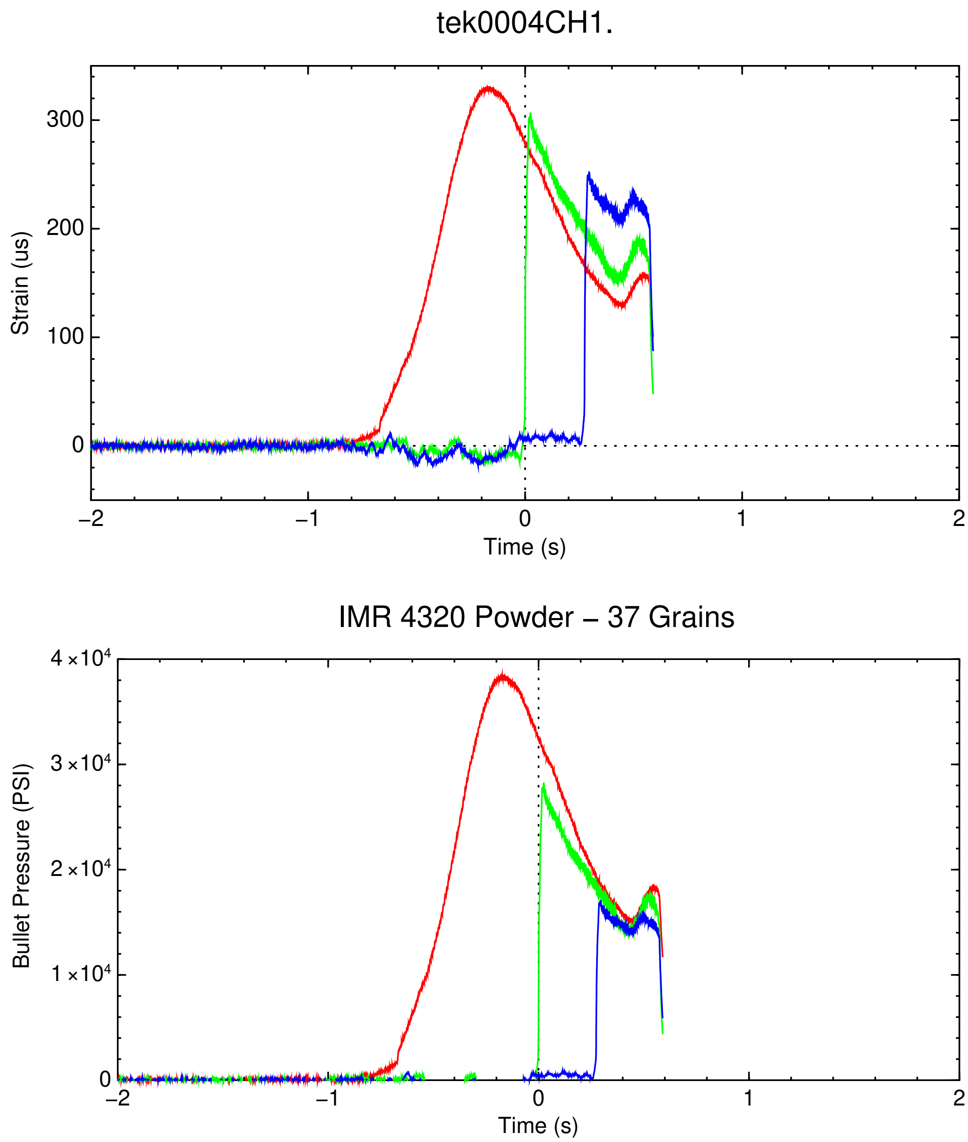

Figure 7: Calculated pressures. Positions from base of case: Red-1.188″, Green-7.443″, Blue-13.653″.

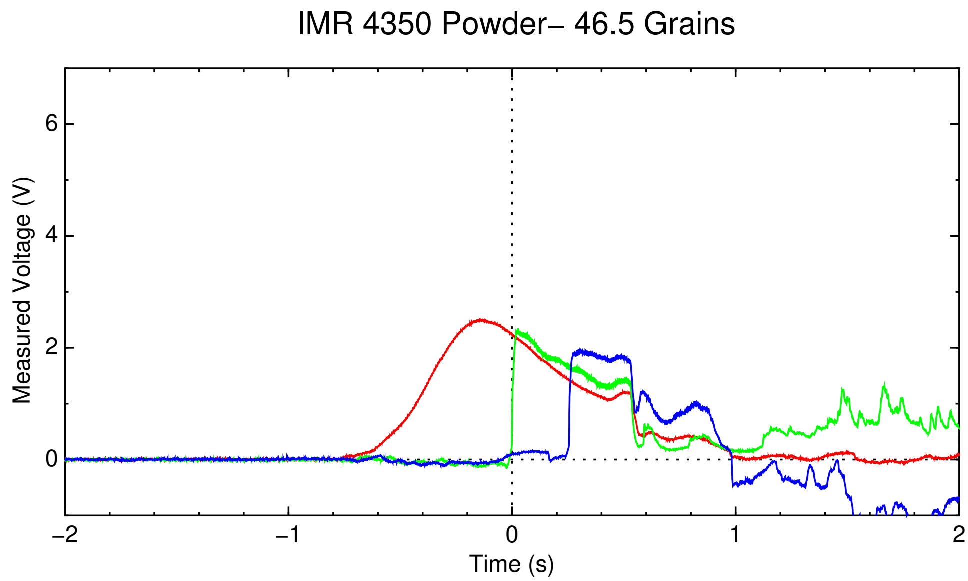

Figure 8: Measured voltages. Positions from base of case: Red-1.188″, Green-7.443″, Blue-13.653″.

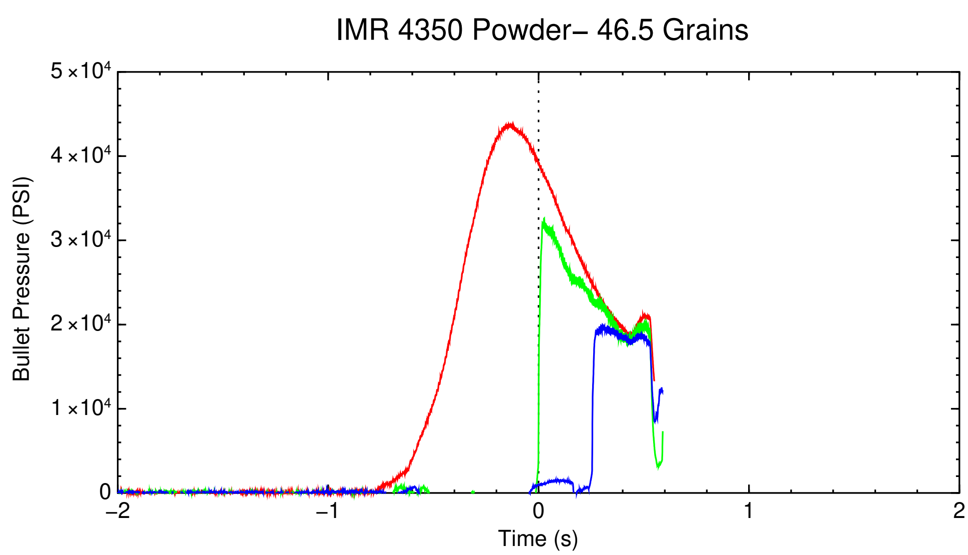

Figure 9: Calculated pressures. Positions from base of case: Red-1.188″, Green-7.443″, Blue-13.653″.

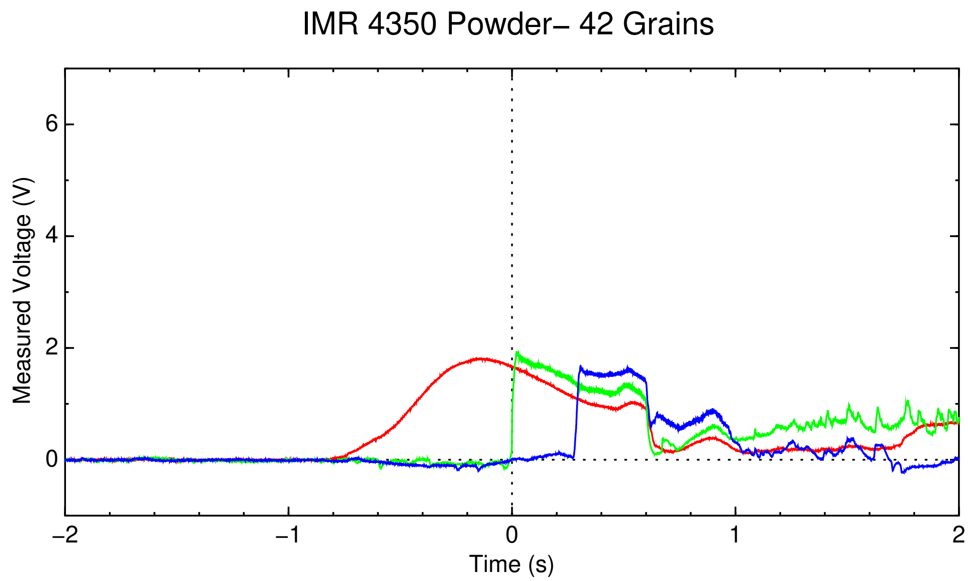

Figure 10: Measured voltages. Positions from base of case: Red-1.188″, Green-7.443″, Blue-13.653″.

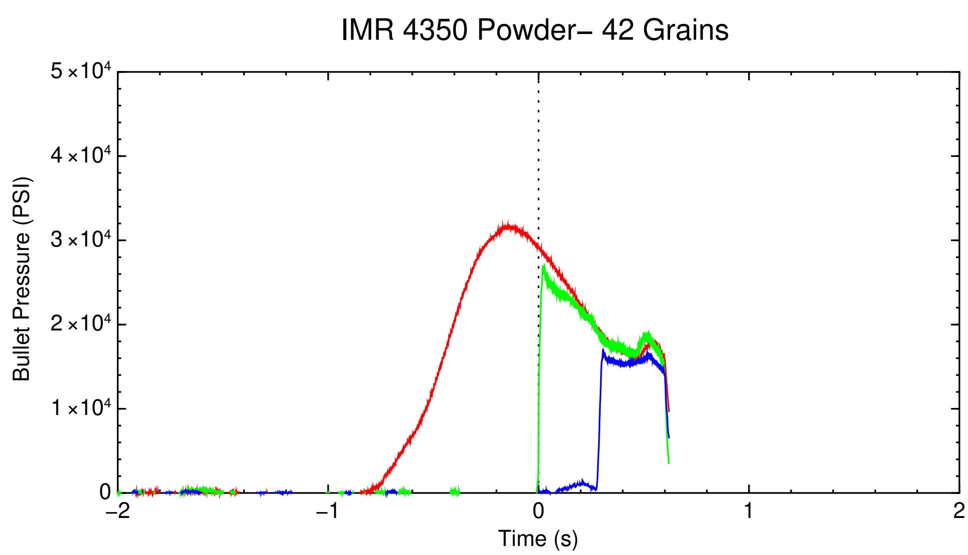

Figure 11: Calculated pressures. Positions from base of case: Red-1.188″, Green-7.443″, Blue-13.653″.

Table 2:

Powder	IMR 4320	IMR 4350	IMR 4350
Weight (grns)	37	46.5	42
Measured velocity (fps)	2427	2598	2368
Starting engraving pressure (psi)	12107	13393	9103
Starting engraving time (ms)	-0.7053	-0.624	-0.798
Arrival time for gauge 2 (ms)	0.	0.	0.
Arrival time for gauge 3 (ms)	.275	.255	.285
Exit time (ms)	.623	.582	.652
Start of bore (in)	3.18 135	3.18	3.18
Position of gauge 2 (in)	7.443	7.443	7.443
Position of gauge 3 (in)	13.653	13.653	13.653

The pressure curves shown in Figures 7, 9 and 11 ideally should overlay one another. The fact that they do not indicates some variation in the measured strain and/or its dependencies. Another potential cause for this behavior is that the temperature along the barrel is not constant as a function of time, resulting in different resistivity behaviors in the strain gauges.

4. Pressure Losses

The energy produced by the powder burned in a cartridge does not all go into accelerating the bullet through the barrel. There are several loss mechanisms that remove some of the available energy as described in [1]. Two loss mechanisms are going to be examined in this report. The first mechanism is the energy to engrave the bullet in the bore. Once the bullet is ejected from case, the bullet circumference is deformed to produce an interference fit with the grooves and lands of the bore. This mechanism requires significant pressure. The next loss mechanism is the kinetic friction the bullet experiences as the bullet transverses along the bore. There are other loss mechanisms such as cartridge expansion, gas heating and unburned powder, which are not of interest here.

Figure 12 is a typical chamber pressure curve for a rifle. This curve illustrates the chamber pressure during the bullet's motion through the barrel. There are two features of interest in this curve. The first feature is a "kink" in the curve occurring at -.6716 ms. This small but rapid change of pressure is attributed to the bullet being positioned into the lands and grooves of the bore after it is ejected from the case hitting the bore. The chamber pressure at this time is consistent with the pressure required for the bullet to be ejected from the neck of the cartridge.

The required pressure to eject a bullet from a cartridge can be estimated by measuring the compression required to seat a bullet in a case. A compression measurement was performed using a Mark-10 force meter [4]. The measured insertion force was 134 lbs (2100 psi), which is comparable to the observed pressure at what is termed Feature 1 in Figure 12.

At this point, the bullet is at the beginning of the bore, being forced into the bore and making a tight gas seal with the bore. As the pressure increases, the bullet is forced completely into the bore. There is another feature in the pressure curve that indicates when the bullet starts to enter the bore. Note that at -.5176 ms, there is a slight change of slope in the pressure curve ($\sim$12k psi/760 lbs).

To better appreciate the pressure of forcing a bullet through a barrel, a mechanical bullet pusher test fixture was made. Mechanical bullet push testing has been done by others [2]. This test fixture allowed for the measurement of the amount of force required to push a bullet through the bore of a barrel as a function of position. Figure 13 illustrates the test fixture. This figure is a collage of four images illustrating a unique section of the test

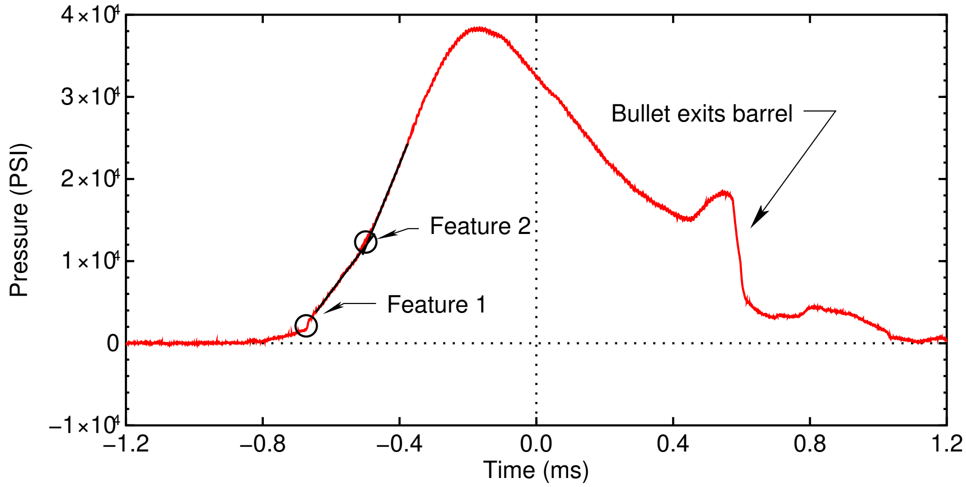

Figure 12: Illustration of a typical chamber pressure curve.

fixture. The lowest section is on the left and continues to the highest section on the right.

The image on the left is a manually pumped hydraulic jack used to push the bullet through the bore. A calibrated load cell was used to measure the applied force. The load cell calibration used the Mark 10 force meter as a reference. The load cell was positioned between the hydraulic jack and a .25″ diameter rod. The rod was guided by wood plates to keep the rod collinear. The other end of the rod was machined to a 5/32″ diameter for a 5/32″ length. This machined end was inserted into a drilled hole at the base of the bullet. The details of this interface are illustrated in Figure 14.

The bullet position was measured using a linear encoder mounted to the left of the rod as illustrated in the second image on the left in Figure 13. The linear encoder was connected to the rod assembly. The linear encoder assembly was adjusted to position the bullet at the lands at the start of the measurement. As the bullet was pushed in the barrel, PCV columns were removed from the rod/column assembly, which helped to maintain alignment. A nylon bushing was also used to maintain alignment as shown in Figure 15.

Figure 16 illustrates the typical results for mechanically pushing a Hornady Interlock 7mm BTSP 139 grain bullet. The oscillations are due to manually pumping the hydraulic jack. This manually pumped hydraulic jack could not maintain the pressure between strokes. A motorized, hydraulic pump would have been ideal to use in this application since a continuously increasing pressure could have been applied. The peak measured pressure had some variation between different test runs. This could be due to initial alignment of the bullet in the lands. Misalignment might be minimized in an actual firing since the generated pressure would tend to self-align the bullet in the lands.

Figures 17 and 18 are the resulting measured force and resulting equivalent pressure (force/area) when the peak pressure values from Figure 16

Figure 13: Bullet pusher test fixture illustrated in four sections.

are used. The curves in Figures 17 and 18 have an under sampled/choppy appearance since a continuous increasing pressure could not be applied using a manual, hand-pumped hydraulic jack. The plotted values were the peak measured pressure for each handle pump. The piston displacement was about .375″ for each pump stroke. Figure 19 illustrates the engrave markings on a bullet from the lands.

5. Equations of Motion

The position and velocity, r and v, respectively, of a bullet can be calculated using the classical equations of motion, which are

$$v = a * t + v_0 \tag{1}$$

and

$$r = r_0 + v_0 * t + .5 * a * t^2 \tag{2}$$

Figure 14: Bullet/rod connection.

Figure 15: Illustration of nylon bushing to assist in keeping coaxial alignment of the pushing rod.

where t is time, a is the acceleration and v_0 and r_0 are the initial velocity and position values. The acceleration is directly related the chamber pressure as

$$a = (\text{area}/m) * p \tag{3}$$

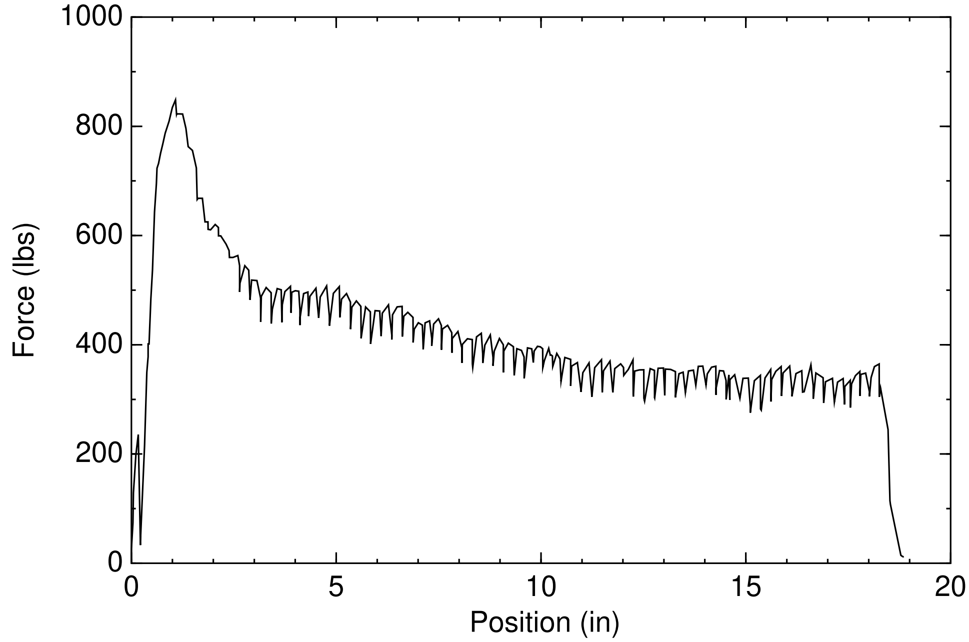

Figure 16: Measured force for mechanically pushing a Hornady Interlock BTSP bullet though a 7mm barrel.

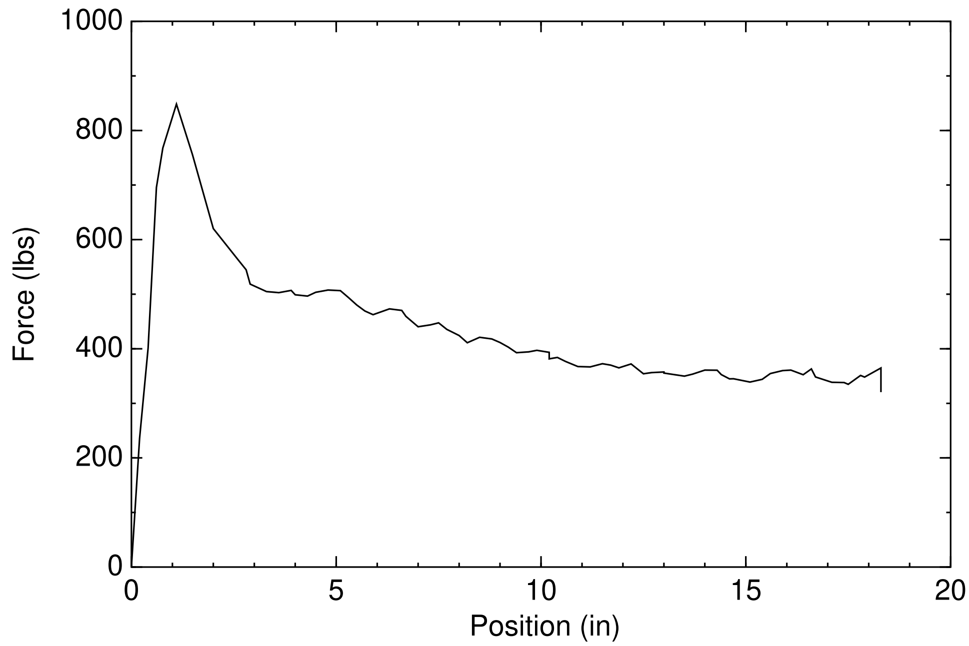

Figure 17: Engraving force for a Hornady Interlock BTSP bullet being mechanically pushed through 7mm barrel.

where area is the cross sectional area of the bullet, m is the mass of the bullet and p is the chamber pressure. Note that the mass is given by 139/7000/32.174, where 7000 is the number of grains in a pound and 32.174 is the number of slugs in a pound.

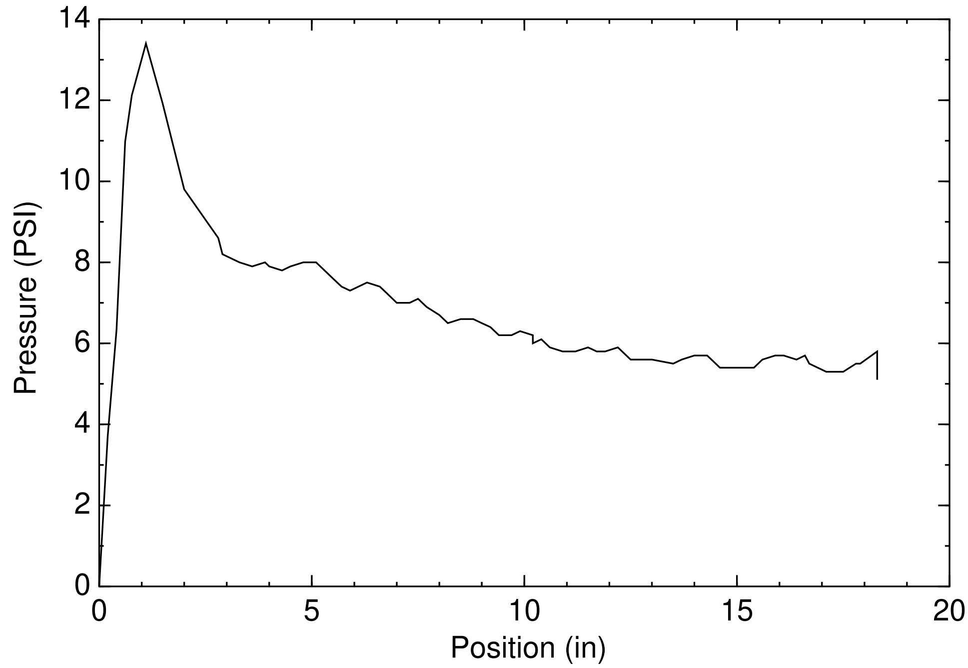

Figure 18: Engraving pressure for a Hornady Interlock BTSP bullet being mechanically pushed through a 7mm barrel.

Figure 19: Illustration of engraved bullet after being pushed through the whole bore length.

Numerically, these equations can be coded as

```
con=area/m
do i=i_s,i_e-1
   vel(i)=0.
```

```
      len(i)=0.
      if(i.ge.i_en) then
         accel_ave=con*(p(i)-press_loss)
         dvel=accel_ave*dt
         len(i)=len(i-1)+vel(i-1)*dt*12.+.5*dvel*dt*12.
         vel(i)=vel(i-1)+dvel
         if(p(i).le.press_loss .and. p(i-1).gt.p(i)) then
            istop=i
            goto 10
         end if
      end if
   end do
10 continue
```

where $p(i)$ is the chamber pressure found in Equation B.9 (Appendix B) and $press\_loss$ is the equivalent pressure loss of the drag/friction of the bullet moving through the barrel. As described below, two different pressure loss functions were used in this study.

Figure 20 illustrates the three measured chamber pressure profiles used in the numerical modeling. They have been smoothed with a moving average of 21 pts and the trailing portion has been modified to remove the measurement artifacts during the time the bullet exits the barrel. The modification entailed a linear extension of the pressure curve. The symbols on the curves represent the location of the two characteristic features referenced in Figure 12 and the two points used to extend a linear extrapolation of the chamber pressure curves to zero.

6. Pressure Loss Calculations

The static (engraving) and kinetic friction forces were found using a numerical downhill simplex optimizer. The optimizer found the effective forces (pressures) by matching the calculated velocity to the muzzle velocity. The measured muzzle velocities were obtained using a chronograph. The optimized functional was

$$abs(v_{cal} - v_{mea}). \tag{4}$$

An alternate functional could have been based upon bullet travel such as

$$abs(r_{cal} - r_{mea}). \tag{5}$$

where r_{mea} is the length of the bore plus the length of the bullet that has a .284″ diameter.

Two different pressure loss functionals were used for these calculations. Each functional had one parameter that the optimizer was searching for. The first functional used was a constant and the second functional used was

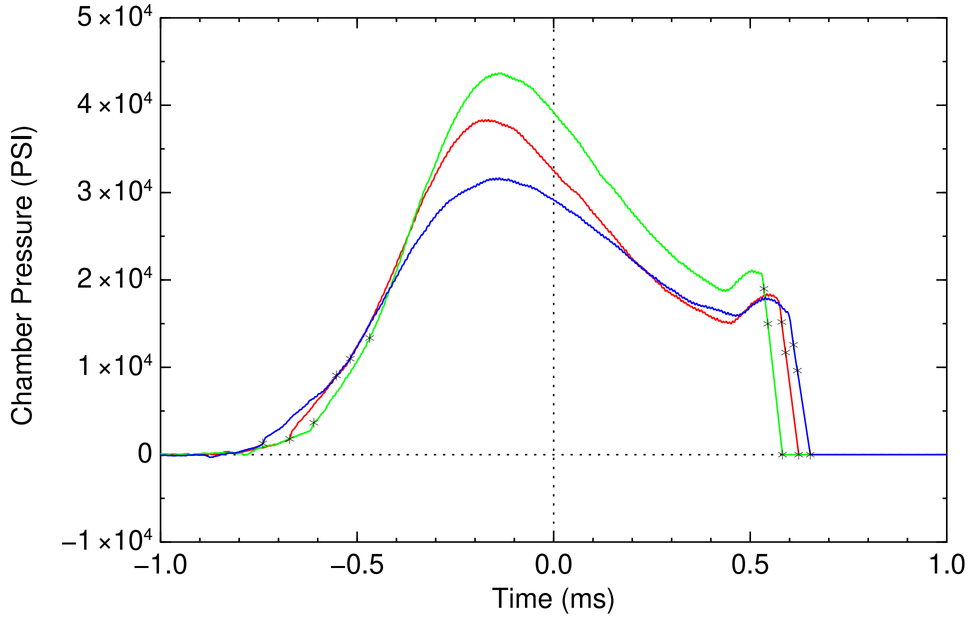

Figure 20: Chamber pressure curves used in the numerical modeling symbols showing points of interest. Red-IMR 4320, 7 grains; Green-IMR 4350, 46.5 grains; Blue-IMR 4350, 42 grains

a scaled version of the chamber pressure. The scaled functional was formed by subtracting the pressure at the start of the engraving process and the resultant was then scaled. These functionals can be described as

$$\text{functional 1} : press\_loss = constant \tag{6}$$

and

$$\text{functional 2} : press\_loss = (p(t) - p\_en) * scale \tag{7}$$

where $p(t)$ is the chamber pressure as a function of time and p_en is the chamber pressure at the start of the engraving process.

Using a scaled version of the chamber pressure for a pressure loss functional may not be unreasonable since it is the resistance of the bullet traveling through the bore that generates the chamber pressure profile. The optimizer determines what the constant value and the scale factor have to be to achieve a calculated muzzle velocity to match the measured muzzle velocity.

Table 3 tabulates the calculations for the three loads and two different loss functionals. Note that calculating the average pressure loss from the scaled functional yielded a value close to the constant functional value. The calculated bullet path length in the bore was close to the actual bore length.

Table 3 also provides comparisons for two internal, average bullet speed values. The first average speed is over the distance from the bore lands to the second strain gauge and the second average speed is over the distance from the second strain gauge to the third strain gauge. The measured times for the bullet to traverse these two distances is acquired from the oscilloscope data. These speeds are average speeds since they are determined from the time it takes a bullet to traverse these distances.

Comparable speeds over these two distances are also numerically determined. The two calculated average internal speeds are slightly smaller than the measured speeds. This could be caused by that the calculated pressure loss initially being too large provided that the calibrated chamber pressure from the strain gauge measurements is too small. To address the later possibility, the chamber pressure values were artificially scaled to larger and smaller values to observe if the calibrated chamber pressures from the strain gauge measurement were off. No improvement in matching the measured and calculated average speeds was observed. This suggests that the initial pressure loss is too large.

Table 3:
Calculated internal ballistics data for a 7x57mm Mauser

Powder	IMR 4320	IMR 4350	IMR 4350
Weight (grns)	37	46.5	42
Measured velocity (fps)	2427	2598	2368
Measured bore length (in)	18.85	18.85	18.85
Constant pressure loss (psi)	4218	5500	3156
Constant pressure loss (lbs)	267	348	199
Measured average speed 1	632	729	609
Calculated average speed 1	597	641	544
Measured average speed 2	1885	2018	1799
Calculated average speed 2	1880	2021	1779
Final distance (in)	18.56	18.07	18.34
Scale factor for second functional	.2114	.2366	.1750
Average pressure loss	4202	5466	3128
Measured average speed 1	632	692	574
Calculated average speed 1	583	624	527
Measured average speed 2	1885	2018	1799
Calculated average speed 2	1819	1945	1731
Final distance (in)	18.66	18.23	18.65

Figures 21 through 23 illustrate the calculated speed and position for the bullet when the load consisted of IMR 4320 at 37 grains. The other two loads had similar behavior. Note that when the chamber pressure is plotted as a function of distance and not time, as it was measured, the pressure variation has a similar profile to that of the mechanical bullet push data shown in Figure 18. This suggests that using a scaled version of the chamber pressure was a reasonable approximation for the pressure loss due to the bullet/bore friction.

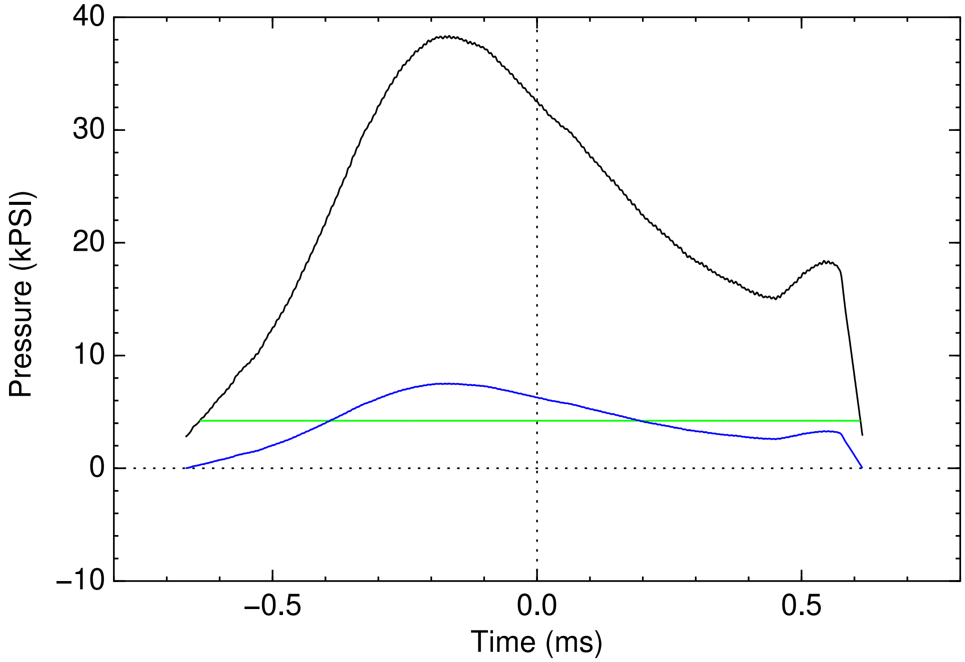

Figure 21: Calculated pressure loss and measured chamber pressure for 37 grns of IMR 4320 as a funcition of time. Black: Chamber pressure, Green: constant pressure loss, Blue: scaled loss pressure.

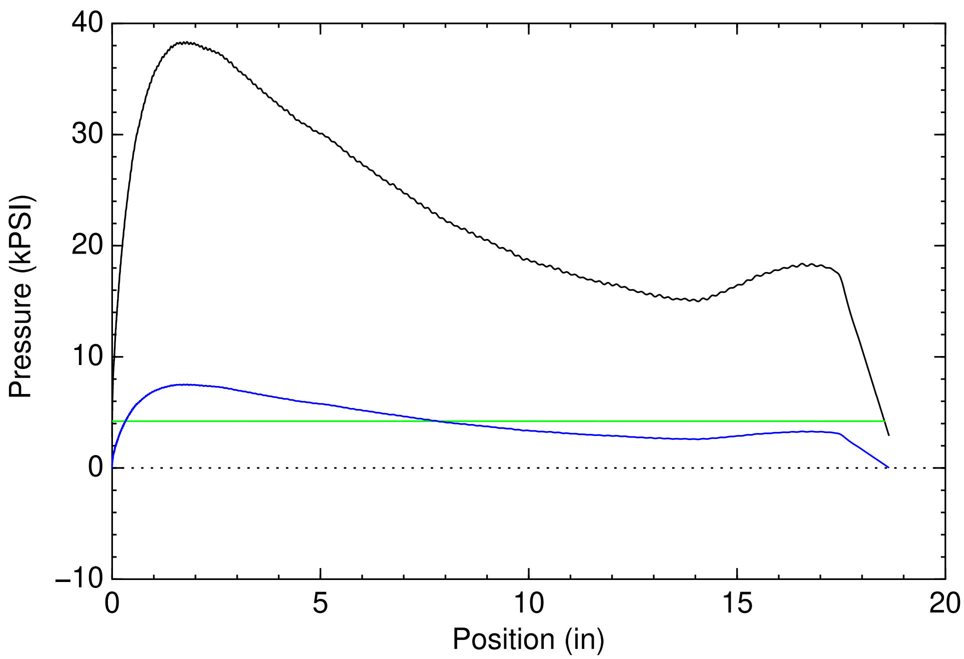

Figure 22: Calculated pressure loss and measured chamber pressure for 37 grns of IMR 4320 as a function of distance. Black: Chamber pressure, Green: constant pressure loss, Blue: scaled loss pressure.

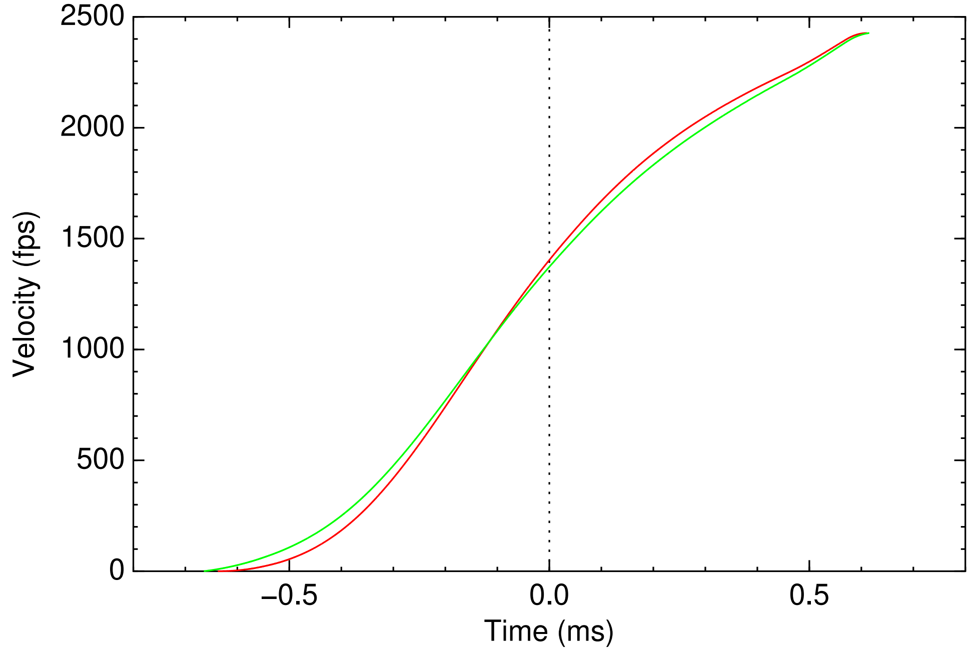

Figure 23: Calculated bullet velocity in the Mauser barrel. IMR 4320, 37 grns as a function of time. Green: constant pressure loss, Red: scaled loss pressure.

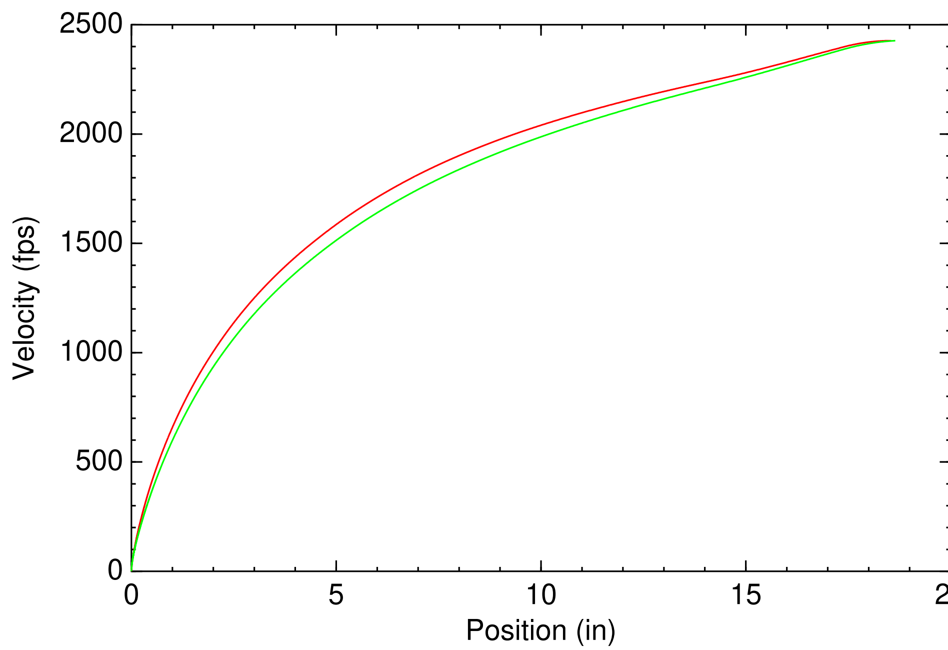

Figure 24: Calculated bullet velocity in the Mauser barrel. IMR 4320, 37 grns as a function of distance. Green: constant pressure loss, Red: scaled loss pressure.

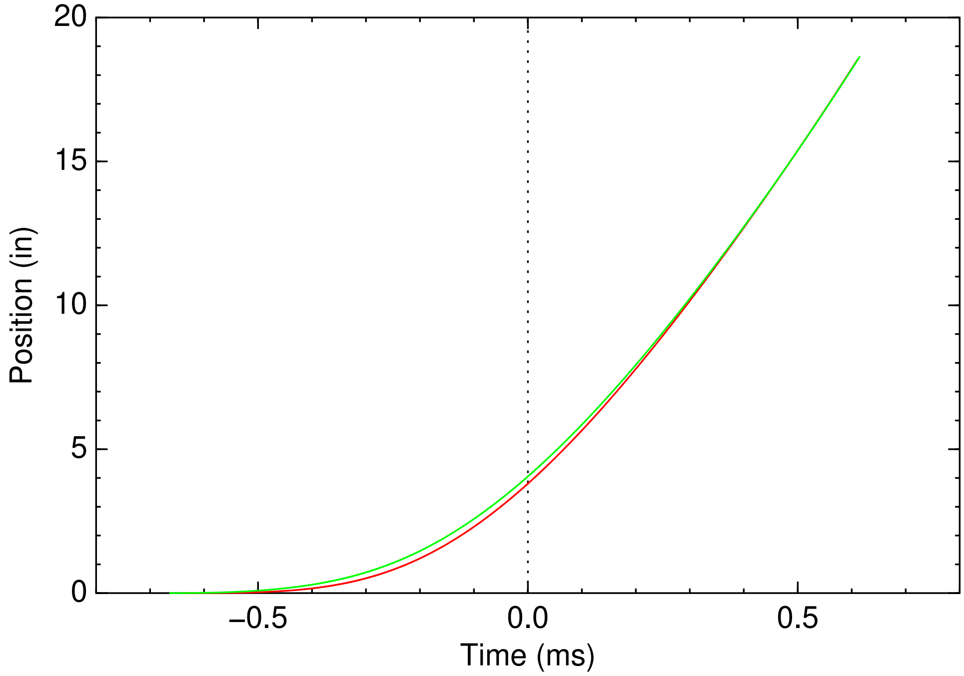

Figure 25: Calculated bullet position in the Mauser barrel. IMR 4320, 37 grns. Green: constant pressure loss, Red: scaled loss pressure.

Figure 26 is a comparison of pressure loss functionals. All of them have similar trends. The calculated functionals tend to have comparable pressure losses near the muzzle end of the barrel. This is satisfying since the kinetic drag should be similar. However, the calculated functionals have different losses near the chamber end of the barrel. This may be reasonable since the larger pressure losses are associated with the faster muzzle speeds (higher initial acceleration) and a faster engraving process requires more force.

A typical pressure loss from the mechanical bullet push test is also shown in Figure 26 (magenta curve). These pressure loss values are much larger than the calculated pressure loss values. There are two potential explanations for this. Several push tests were performed and even though care was taken to properly align the bullet in the lands, the peak force did very. It is believed that the alignment variation caused different peak values. In an actual cartridge firing, the uniform pressures in the chamber could align the bullet fairly well. A second explanation for the higher pressure losses could be that the loss is a function of the bullet's speed/acceleration.

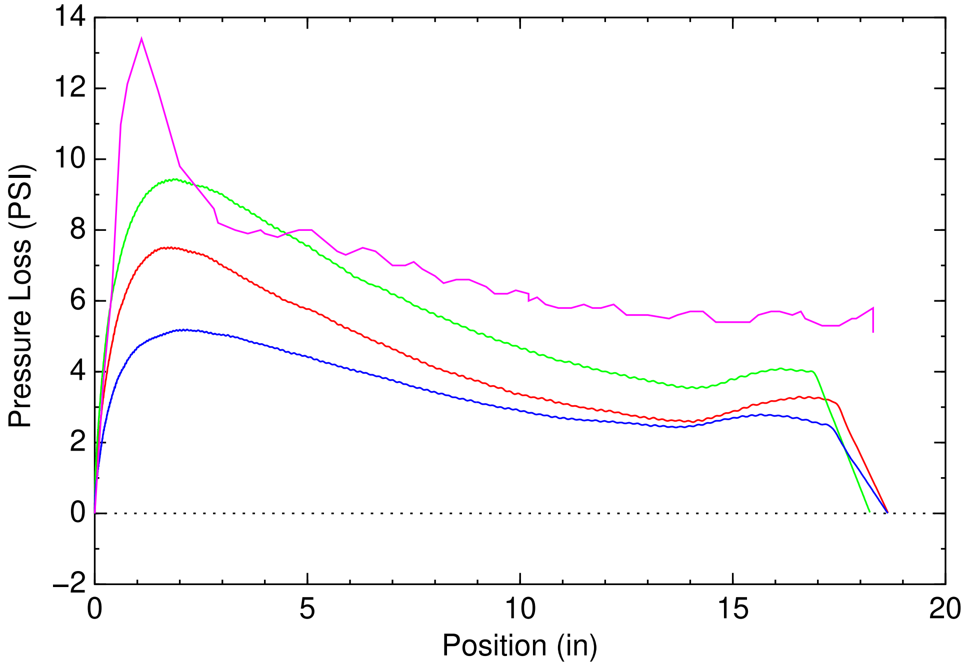

Figure 26: Comparison for pressure loss functionals for the three loads and mechanical push test. Red: IMR 4320-37 grains, Green: IMR 4350-46.5 grains, Blue: IMR 4350-42 grains, Mageneta: push test.

7. Conclusions

It is desirable to be able to provide as much pressure as possible to accelerate a bullet in a barrel. For a given case, powder load and barrel tensile strength, there is a limit to how much pressure can be generated. Having the ability to determine these friction forces, or their effective pressure losses, may provide a figure of merit for various bullet and bore designs.

Three analytic approaches were examined in this report to gain information on the loss forces. The first one was providing additional information on bullet travel along the length of the bore using multiple strain gauges. This provided timing information on how fast the bullet was traveling between the actual measurement locations. This provides guidance on performance but limited insight on improving the performance.

The second approach examined the pressure loss caused by bullet/bore friction during and post the engraving process. Two different pressure loss profiles (constant and scaled), were used with the scaled pressure loss functional being the most accurate. This approach provided additional information regarding the speed and location of the bullet as a function of time.

The third approach was to mechanically push a bullet through a barrel's bore and measure the required force. It was observed that a similar result was obtained to the second approach with the scaled functional. The benefit of this approach was that a firing was not required but it was observed that bullet alignment during the initial engraving process is critical. This could limit the usefulness of mechanically pushing a bullet through a bore. Note that the second approach also allows the impact of powder performance to be considered.

Two potential features of the chamber pressure curves, were highlighted in this article. One of them apparently was related to the start of the engraving process as the bullet enters the barrel. The second feature had a slight change in the slope of the chamber pressure profile. The cause of this feature could not be resolved or identified. This slope change occurred about .080″ from the start of the of the bore. Perhaps the bullet at this point provided a sufficient seal with the bore to retain the powder gases more efficiently, which is why the rate of pressure increase became larger.

Additionally, it is believed that the calibration of the measured strain gauge voltages to obtain pressure levels was reasonable since the internal ballistic calculations agreed with independent measured values.

8. Acknowledgments

The authors would like to thank Jim Caudill and Jeff Siewert. Jim provided the use of his property to perform these measurements. Without access to this location, it would have been difficult to collect the data used in this report. Jeff provided a sanity check on the interpretation of the pressure curves.

Appendix A. Wheastone Bridge

The barrel pressure can be inferred by using a strain gauge which changes its electrical resistance due to small physical compressive or expansive forces that the supporting surface experiences [5, 6, 7]. Strain gauges have been used for many years to measure deformations. One early study is found here [8]. A commercially available strain sensor system is available from Recreational Software, Inc. (RSI) [6]. Additional information on sensor preparation and measurement technique is available at [7].

The change of the electrical resistance is small, so a sensitive circuit has to be used to measure this small change. One circuit capable of this measurement is called a Wheatstone bridge. There are a number of different Wheatstone bridge configurations available [9] to measure small resistive changes. Figure A.27 illustrates the typical resistive network. It consists of three additional resistors with the strain gauge.

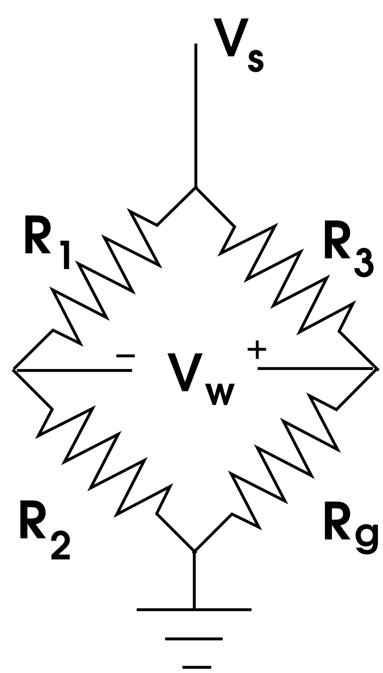

Figure A.27: Basic Wheatstone bridge.

When $R_1/R_2 = R_3/R_g$, the bridge is balanced meaning the voltage at V_W is zero. When there is strain placed on the sensor (R_g), the resistance of the sensor changes and this voltage is no longer zero since the bridge is no longer balanced. It is this voltage that is measured to obtain the pressure inside the chamber. The expression which relates voltage to strain is given in Equation A.1 [9]

$$\epsilon = \frac{4V_w'}{\mathrm{GF}(1 - 2V_w')} \tag{A.1}$$

where ϵ is the strain, V'_w is the normalized measured Wheatstone bridge voltage (V_w/V_s) with all the resistors equal ($R_1 = R_2 = R_3 = R$ and $R_g = R + \Delta R$). The factor GF is the gauge factor that has a value of around 2. This value is provided by the gauge manufacturer and is the calibration factor for the gauge relating the normalized resistance change to the strain. The gauge factor is defined as

$$\mathrm{GF} = \frac{\Delta R/R}{\epsilon} \tag{A.2}$$

where ΔR is the resistance change of the strain gauge.

Equation A.1 was derived by expressing the differential voltage as

$$V_w = \left[\frac{R_g}{R_3 + R_g} - \frac{R_2}{R_1 + R_2}\right] V_s \tag{A.3}$$

then setting $R_1 = R_2 = R_3 = R$ and $R_g = R + \Delta R$ and solving for ϵ using the GF relationship in Equation A.2.

When the Wheatstone bridge is physically realized, the sensor is typically physically removed from the other resistors and the impact of having connecting wires should be addressed. Figure A.28 illustrates the electrical model.

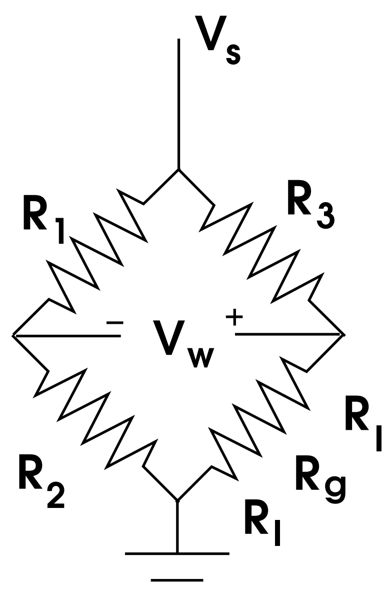

Figure A.28: Wheatstone bridge with sensor wire loss included.

The effect that the wires present is an additional loss component. This loss is very small but so is the resistance change of the sensor due to strain changes. Equation A.1 can be modified to account for this resistance as follows:

$$\epsilon = \frac{4V'_w}{\mathrm{GF}(1 - 2V'_w)} + \frac{4V'_w - 2}{\mathrm{GF}(1 - 2V'_w)}\frac{R_l}{R} \tag{A.4}$$

where R_l is the loss in one connecting wire. In this application, these connecting wires are very short ($\sim$ 6 inches in length) but still significant with respect to the resistance change of the sensor as shown later. For reference, 26 gauge copper wire has about 40 ohms/1000 feet and 30 gauge copper wire has about 100 ohms/1000 feet. This makes R_l .02 ohms for 6 inches of 26 gauge wire and .05 ohms for 6 inches of 30 gauge wire.

Equations A.1 and A.4 can be simplified since the normalized Wheatstone bridge voltage is very small. The loss of accuracy has been numerically confirmed and it is negligible in this application. The maximum normalized Wheatstone bridge voltage for a higher power cartridge is of the order of .5 millivolt so Equation A.4 can be approximated as

$$\epsilon \approx \frac{4V_w'}{\mathrm{GF}} - \frac{2}{\mathrm{GF}}\frac{R_l}{R}. \tag{A.5}$$

However, there is probably no reason to use this approximation with today's numerical calculation resources. It does demonstrate that the strain is primarily given by the first term and that the contribution of loss from the connecting wires to the strain gauge is essentially a constant DC term that is about 100 times smaller than the first term for the given loss values.

There also is a three wire sensor configuration [9] where a second wire is attached to one of the sensor pads. This is only effective at eliminating the loss in one of the wires so it is found not to be helpful and not really of value considering the size of R_l in this application.

Appendix B. Strain-Pressure Relationship

The relationship between the measured strain values to the internal pressure of a chamber is presented here. Approximate expressions can be found in [10]. The author attempted to relate the internal chamber pressure to the external strain on the barrel using expressions for thick and thin walled pressure vessels. The presentation was technically weak and resulted in the use of equations not appropriate for this application. These equations, however, did provide numerical values that were realistic in magnitude. A formulation to calculate the internal pressure of a chamber using measured strain data is presented below. It is a simple model and appears to be reasonable from the experimental testing presented later.

Traditional cylindrical pressure vessels are called "open" or "closed". A person may be tempted to classify a barrel as a "closed pressure vessel" but it is not. A closed pressure vessel has axial stresses induced by the internal pressures of the cylinder since the ends of the cylinder are physically constrained not to move. Also, the classical "closed pressure vessel" has a steady state pressure throughout the cylindrical structure.

A rifle barrel is **not** a closed pressure vessel in the classical sense. Both ends are not mechanically constrained. The muzzle end is free to move. A strain gauge placed axially along the barrel will not sense any significant axial deformation when the round is fired. This means that the barrel can be modeled as an "open pressure vessel". Additionally, the pressure that the barrel is exposed to is transient in nature and not steady state (i.e., the entire barrel is not under a uniform pressure). The pressure wave, generated by firing the round, propagates down the barrel and does not sense the finiteness of the barrel until the pressure wave is at the muzzle. Until then, the barrel appears to be infinitely long. However, when the pressure wave does reach the muzzle, then additional interaction occurs. FEM modeling [11] confirms this simplistic model for early time.

There are a set of equations called Lame equations [12] describing the stresses in a cylindrical structure when the internal and external surfaces are under pressure. These stresses can be grouped into three types: circumferential, axial and radial. The only stress that is of significance when a round is fired in a gun is the circumferential stress.

The circumferential stress equation of interest is

$$\sigma = \frac{p_i - p_o u^2}{u^2 - 1} - \frac{r_i^2 u^2 (p_o - p_i)}{r^2 (u^2 - 1)} \tag{B.1}$$

where p_i and p_o are the internal and external cylinder pressures, $u = r_o/r_i$ is the ratio of the outer and inner cylinder diameters and r is a position between r_i and r_o. This equation is appropriate for what is termed "thick wall", where the cylinder radii are explicitly used.

Equation B.1 can be specialized for two geometries: one for the barrel and one for the casing. In this model, the casing is in contact with the barrel's inner diameter. Such a geometry is typically called "compound cylinders". For the barrel, Equation B.1 yields

$$\sigma_{so} = \frac{p_c 2}{u_s^2 - 1} \quad \text{when } r = r_{so} \tag{B.2}$$

and

$$\sigma_{sc} = \frac{p_c (u_s^2 + 1)}{u_s^2 - 1} \quad \text{when } r = r_c \tag{B.3}$$

where u_s is the ratio of the outer and inner diameters of the barrel where the strain gauge is located and p_c is the contact pressure between the inner diameter of the barrel and the outer diameter of the casing. Equation B.4 is the pertinent equation for the casing

$$\sigma_{bc} = \frac{p_i 2}{u_b^2 - 1} - \frac{p_c (u_b^2 + 1)}{u_b^2 - 1} \quad \text{when } r = r_c \tag{B.4}$$

where p_i is the internal pressure in the casing (barrel) and u_b is the ratio of the outer and inner diameters of the casing. Note that the subscript "s" refers to "steel" which is what the barrel is made from and the subscript "b" refers to "brass" which is what the cartridge is made from.

The desired equation to predict the interior pressure in a barrel by the measured strain on the exterior of a barrel is derived in two steps. The first step is to relate the change of circumference at the contact interface between the barrel and casing when a round is fired. Since both the barrel and casing are in contact during firing, both have to expand the same amount. This expansion is governed by the strain at the interface and has to be continuous at the contact boundary which requires

$$\epsilon_{bc} = \epsilon_{sc}. \tag{B.5}$$

The strain and stress of a material are related through a constant called Young's modulus or the modulus of elasticity, E, and is expressed as

$$\epsilon = \frac{\sigma}{E}. \tag{B.6}$$

Using Equations B.3 and B.4 with Equations B.5 and B.6 yields

$$p_i = \left[\frac{E_b}{E_s} \frac{u_s^2 + 1}{u_s^2 - 1} + \frac{u_b^2 + 1}{u_b^2 - 1} \right] \frac{u_b^2 - 1}{2} p_c \tag{B.7}$$

where the Young's modulus for steel (E_s), brass (E_b) and LDPE (shotgun shells) are $30 * 10^6$, $16 * 10^6$ and $.13 * 10^6$ psi, respectively. The contact pressure is determined by the strain gauge reading. Using Equations B.2 and B.6 yields this contact pressure which is

$$p_c = \frac{E_s}{2}(u_s^2 - 1)\epsilon_{so}. \tag{B.8}$$

Inserting p_c from Equation B.8 into Equation B.7 and reducing yields

$$p_i = \frac{1}{4} \left[E_b(u_s^2 + 1)(u_b^2 - 1) + E_s(u_b^2 + 1)(u_s^2 - 1) \right] \epsilon_{so}. \tag{B.9}$$

The accuracy in determining the chamber pressure is dependent upon many factors. From Equations A.4 and B.9, the factors are the measured Wheatstone bridge voltage (dependencies of strain gauge bonding/orientation, the gauge factor and amplifier gain), measured chamber/casing dimensions and the Young's modulus material constants. The only factors in which there are known uncertainties are the strain gauge bonding quality to the barrel and the Young's modulus values.

The dimensions used in Equation B.9 should be the dimensions under pressure. Fortunately for the amount of strain on the barrel, the change of the barrel dimensions under pressure is negligible. However, this is not the case for the casing. The outer diameter for the casing should be the inner diameter of the chamber since the case is in contact with the barrel during firing. This results in a thinner case thickness during firing than the case has under static conditions. The case thickness used in Equation B.9 is scaled from the unfired case thickness. This scaling is based upon the fact that the amount of brass is constant. The thickness used is given by $t_2 = r_1 t_1 / r_2$

where the subscripts 1 refer to the dimensions before firing and 2 refer to the dimensions during firing. The change is negligible since the casing diameter expands roughly .004″.

Appendix C. Amplifier Design

Modern opamp capabilities allow for very simple circuits to be made with superior electrical performance. Figure C.29 illustrates one circuit that can measure the differential voltage generated by a Wheatstone bridge. There are two amplifiers used in this circuit. The first amplifier is a Texas Instruments INA129 instrumentation opamp, a device which measures and amplifies the generated differential voltage created by the sensor and rejects the common mode voltage of the balanced bridge. The second amplifier is a Texas Instruments OPA320 opamp which provides additional gain and filters higher frequency noise from the measured signal.

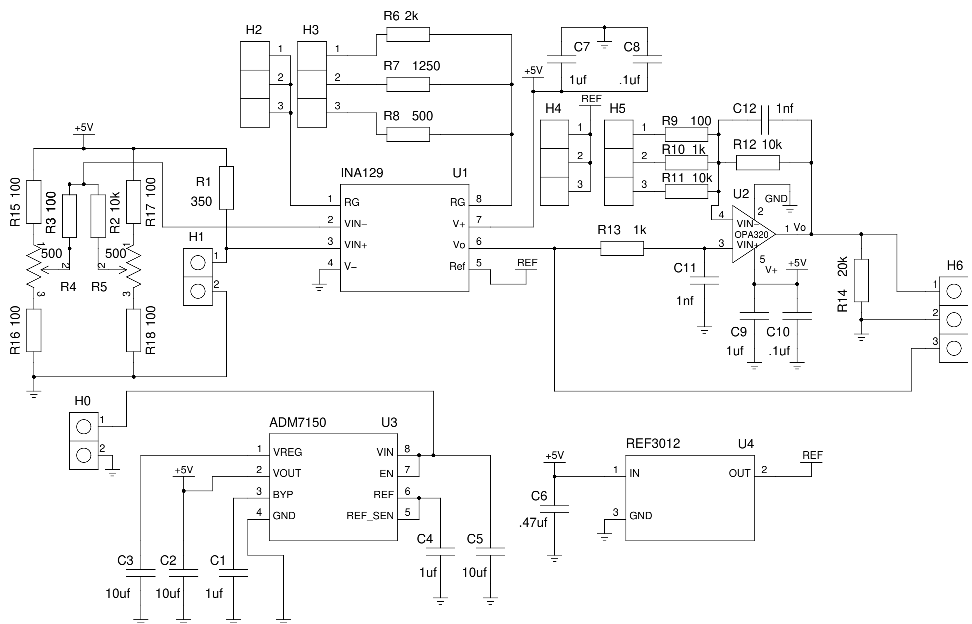

Figure C.29: Schematic for the Wheatstone measurement circuit.

The INA129 has the capability to have an adjustable gain through the choice of resistors R6/R7/R8. This is important since different measurement locations and loads will have different pressure maximums. The gain is defined by $1 + 49.4\text{k}/R$ where R is either $R6$, $R7$ or $R8$. Voltage gains of 25.7, 40.52 and 99.8 are provided when the resistance is 2000, 1250 and 500, respectively. Of course, the actual gain should be measured to obtain the most accurate value for the gain.

The OPA320 has the capability to have an adjustable gain through the choice of resistors R9/R10/R11. The gain is defined by $1 + R12/R$ where R is either $R9$, $R10$ or $R11$. Voltage gains of 101, 11 and 2 are provided when the resistance is 100, 1000 and 10,000, respectively.

The required gain can be estimated by using the expected pressures and strain voltages along the length of a barrel. The values shown in Table C.4 for a 7mm Mauser rifle are derived by using Equations B.7 and B.8.

Table C.4:
Calculated Wheatstone Voltages

Location	u_s	p_i (kpsi)	$\epsilon * 10^6$	V_w (mV)
A	2.5	36	309	.159
B	2.6	27	293	.151
C	2.3	15	226	.116
D	2.0	13	283	.145

The circuit has two jumpers to allow appropriate gains to be chosen. These jumpers select one of three resistors to be used for each amplifier stage. Table C.5 illustrates the various gains possible.

Table C.5:
Gain Combinations

Resistor Selection	Theoretical Gain
R6-R11	51.4
R7-R11	81
R8-R11	199.6
R6-R10	282.7
R7-R10	445.7
R8-R10	1097.8
R6-R9	2595
R7-R9	4092
R8-R9	10079

All the components operate on a 5 volt rail supplied by a 9 volt battery (for portability) and a linear voltage regulator ADM7150. REF3012 provides an offset voltage for the instrumentation opamp's output. Since the generated Wheatstone bridge voltage will be positive (as configured), it is necessary to offset the opamp output by a small voltage when the bridge is balanced. This is achieved by offsetting the INA129 output voltage by 1.2 volts using REF3012. The gain and offset voltage should be set so that the maximum output voltage is less than 4.5 volts for maximum sensitivity.

The circuit uses two multi-turn potentiometers, R4 and R5, to balance the bridge when the sensor has no strain on it. R4 provides coarse adjustment while R5 provides fine adjustment. This adjustment is made to have the output voltages (pins 1 or 3 on H6) the same voltage as the reference voltage from REF3012. This voltage is on all the H4 pins.

A number of connection points (H0-H6) are present. H0 provides for the connection of the 9V battery. H1 is the connection point for the strain sensor. H6 is a measurement point for both the pre-filtered (pin 3) and filtered (pin 1) amplified voltage. Jumpers H2-H3 permit the selection of resistors R6-R8 to be chosen for the INA129 amplifier and jumpers H4-H5 permit the selection of resistor R9-R11 to be chosen for the OPA320 amplifier.

Note that the measured voltage value used in Equation A.1 has to be divided by the total gain of the opamp circuit to recover the Wheatstone bridge voltage.

Appendix D. Velocity-Position Equations

The velocity of the bullet and its position along the barrel can be estimated once the pressure in the chamber has been acquired. Note that the following derivation is under ideal conditions that are not always met in a real life gun chamber/barrel.

The force acting on a bullet is the gas expansion created by the burning of the powder. Considering Newton's Second Law of Motion as was done in [13], the bullet's motion can be roughly modeled by equating its mass and acceleration to the chamber pressure over its cross sectional area as

$$ma = PA \tag{D.1}$$

where m is the mass of the bullet, a is the acceleration, P is the chamber pressure and A is the area of the bullet. Expanding the a as the second time derivative of position yields

$$md^2x/dt^2 = PA \tag{D.2}$$

since

$$a = d^2x/dt^2. \tag{D.3}$$

Realizing that

$$dx/dt = v \tag{D.4}$$

results in Equation D.2 becoming

$$mdv/dt = PA. \tag{D.5}$$

Multiplying both sides with dt and integrating yields

$$m\int_{v1}^{v2} dv = A\int_{t1}^{t2} Pdt \tag{D.6}$$

where $v1$ and $v2$ are the velocities of the bullet at times $t1$ and $t2$, respectively. The integration approach used in [13] is basically wrong. I feel that there is no value in defining an average pressure as was done and the velocity of the bullet is not linear so one cannot say that

$$m \int_0^{v_p} v dv = m \frac{1}{2} v_p^2. \tag{D.7}$$

What can be determined by using Equation D.6 is the velocity and position as a function of time by piece-wise integrating this equation. This is readily achieved since the measured data would be sampled with small, uniform temporal spacings. The velocity is determined by

$$v_i = v_{i-1} + \Delta v \tag{D.8}$$

where $\Delta t = t_i - t_{i-1}$ and $\Delta v = \frac{A}{m}(p_i + p_{i-1})/2 * \Delta t$ and the position is determined by

$$x_i = x_{i-1} + v_{i-1} * \Delta t + .5 * \Delta v * \Delta t. \tag{D.9}$$

The initial values for velocity and position are both zero. The final velocity is the muzzle velocity of when the bullet exits the barrel and the final position is the length of the barrel's bore. The bullet starting location is when the bullet has completely entered the bore.

There is one last consideration to make before calculating velocities and travel distances which is the resistance the bullet experiences traveling through the barrel. There are two types of resistance to account for. One resistance is the bullet engraving process as the bullet is deformed to make an interference fit with the barrel's bore creating a gas tight seal. The other resistance is the friction provided between the bullet and the bore as the bullet moves along the bore. This resistance is less than the engraving resistance.

The energy used to overcome these resistances can be calculated by determining the required pressure to overcome the resistances. Then energy is determined by the force (pressure*area) over the distance the resistance occurs. The distance for the engraving resistance is the length of the contact between the bullet and the bore.

References

[1] Sequard-Base, J., Haas, T., Tomastik, Vernes, A., Franek, F., "Barrel Friction in Sport Rifles", Tribology Letter (2018) 66:3.

[2] White, L., Siewert, J., "Final Report of the Rifling Profile Push Test", Arrow Tech Associates, S. Burlington, VT under contract W911QX-05-P-0451, Army Research Laboratory.

[3] Micro-Measurements (Division of Vishay Precision Group), Raleigh, North Carolina.

[4] Mark-10, https://www.mark-10.com/instruments/stands/tsb100.html.

[5] Strain Gauge, https://en.wikipedia.org/wiki/Strain_gauge.

[6] Recreational Software, Inc., https://www.shootingsoftware.com/pressure.htm.

[7] Strain Gauges for Chamber Pressure Measurements, http:www.ktgunsmith.com /straingauge.htm.

[8] Brownell, L.E., York, M., Sinderman, R., Jacob, K., Robbins H., "Absolute Chamber Pressure In Center-Fire Rifles", The University of Michigan, Industry Program of the College of Engineering, June, 1965, IP-710, https://deepblue.lib.umich.edu/bitstream/handle/2027.42/3866/bac6873.0001.001.pdf?sequence=5.

[9] Quarter Bridge, Half Bridge and Full Wheatstone Bridge Strain Gauge Load Cell Configurations, Transducer Techniques, https://www.transducertechniques.com/wheatstone-bridge.aspx.

[10] Strain Formulas, http://www.mindspring.com/∼sfaber1/strnform3.htm.

[11] 22LR Rifle and Tuner, http://www.varmintal.com/a22lr.htm.

[12] Thick wall stress formulas. http://www.engineeringtoolbox.com/stress-thick-walled-tube-d_949.html.

[13] Calculating Barrel Pressure and Projectile Velocity in Gun Systems, http://closefocusresearch.com/calculating-barrel-pressure-and-projectile-velocity-gun-systems.

[14] GS Custom Bullets, http://gscustom.co.za/.